JOURNAL OF MATERIALS SCIENCE 29 (1994) 6403–6412

TEM study of metastable β-phase decomposition in rapidly solidified Ti–6Al–4V alloy

Z. FAN, A. P. MIODOWNIK
Department of Materials Science and Engineering, University of Surrey, Guildford, Surrey, GU2 5XH, UK

A new rationale is presented for various decomposition products obtained from the metastable β-phase found in Ti–6Al–4V alloy produced by hot isostatic pressing comminuted melt-spun fibres and cooled to room temperature by furnace cooling. This alloy has an α-matrix with about 8 vol% retained β-phase, which is supersaturated with β-stabilizers to such an extent that the martensitic transformation has been suppressed. The metastable β-phase decomposes by different modes during continuous cooling, depending on the actual composition of individual β-grains. Less enrichment of vanadium and iron favours the direct formation of the equilibrium α-phase from the β-matrix, while greater enrichment of vanadium and iron leads to a spinodal decomposition of the metastable β-phase, resulting in a β + β′ two-phase structure. During further continuous cooling, the β′-phase which is lean in β-stabilizers will transform into isothermal ω-phase. In addition, an unknown phase has also been observed in the β-phase, which is typified by the appearance of $1/2\{1\,1\,2\}_\beta$ reflections in the SAD patterns.

1. Introduction

Decomposition of the metastable bcc β-phase in titanium alloys has been investigated for more than three decades [1]. It is well known that a metastable β-phase can be retained in all titanium alloys which are sufficiently rich in β-stabilizers (e.g. iron molybdenum, vanadium, niobium) on quenching from the β-phase field to room temperature. The decomposition of the metastable β-phase can occur by several modes, depending on the alloy system, composition and thermal conditions [1]. When the martensitic transformation is suppressed, the metastable β-phase can decompose either athermally to form an athermal ω-phase upon quenching from the β-phase field, or isothermally to form an isothermal ω-phase on ageing at a low temperature [2]. In alloys which contain a sufficient concentration of β-stabilizers to suppress ω-phase formation, the metastable β-phase will decompose by phase-separation reaction into a solute-lean β′-phase with corresponding solute enrichment of the β-matrix [1, 3]. In addition, the direct formation of the equilibrium α-phase as a product of the metastable β-phase decomposition has also been recognized for a long time [4]. However, all these decomposition modes have not yet been fully integrated in terms of thermodynamic conditions, transformation mechanisms and the correlation among different decomposition modes. There is currently no consensus view in the literature.

In this paper, we report the experimental results on metastable β-phase decomposition in a rapidly solidified Ti–6Al–4V alloy, which has been obtained by hot isostatic pressing of comminuted melt-spun fibres at 900 °C, 300 MPa for 2 h and furnace cooled to room temperature. TEM observation and electron diffraction show that the metastable β-phase in this alloy has decomposed variously by direct formation of the equilibrium α-phase, by spinodal decomposition to form a mixture of β + β′, and by formation of the isothermal ω-phase. In addition, we also report the observation of an unknown phase, which is characterized by the occurrence of $1/2\{1\,1\,2\}_\beta$ reflections in SAD patterns. The relationship between the different decomposition modes and the comparison with the decomposition modes in other alloy systems, are discussed.

2. Experimental procedure

Melting and melt-spinning were performed in a Marko's Model 5T melt spinner in a stainless steel chamber with a high vacuum/inert gas (argon) atmosphere. The alloy was melted in a water-cooled copper hearth using a non-consumable tungsten electrode under a high-purity argon atmosphere. The chemically homogeneous melt was then delivered at a controlled rate to contact the circumferential surface of a molybdenum wheel rotating at 2500 r.p.m. by which the melt is rapidly solidified as long fibres. The melt-spun fibres have a crescent-shaped cross-section, typically 100–300 μm in width and 40–100 μm in thickness. The melt-spun fibres were comminuted into finer particles with particle size less than 200 μm. The comminuted alloy powders were then filled into cylindrical titanium-alloy cans which were baked in the

0022–2461

temperature range 250–300 °C in a vacuum (10^{-5} torr; 1 torr = 133.322 Pa) before they were sealed by electron-beam welding. This procedure was adopted to remove occluded gases in the powder compacts. The cans were consolidated by hot isostatic pressing (HIPing) at 900 °C, 300 MPa for 2 h, and then furnace cooled to room temperature. Further details for preparation of the materials under this study were given elsewhere [5].

Specimens for SEM and EDX analysis were prepared by applying the standard mechanical polishing techniques. Thin foils for TEM study were prepared in a "Tenupol" unit using an electrolyte of 5 vol % perchloric acid in methanol. The polishing temperature was around − 40 °C, the voltage 30 V, the current about 30 μA. TEM observation was performed on a Jeol 200 CX STEM under an accelerating voltage of 200 kV. Energy dispersive X-ray (EDX) analysis was performed on a JXA8600 EPMA system for phase composition.

3. Results

The chemical composition of the master alloy is given in Table I. The results of chemical analysis of the melt-spun fibres and comminuted powders are presented in Table II. The oxygen level has increased after the melt-spinning process, especially after the comminution process, from 2050 p.p.m. in the master alloy to 3100 p.p.m. in the comminuted alloy powder. The oxygen content in the HIPed alloy is just slightly higher than 3100 p.p.m. due to the good vacuum level in the HIPing process.

The microstructure of the consolidated Ti–6Al–4V alloy is shown in Fig. 1 by a SEM secondary electron image. The α-phase (grey) has an equiaxed morphology with an average grain diameter of about 6 μm, while the β-phase (white) has an irregular shape and is located at α-grain boundaries and α-grain triple points. The volume fraction of the β-phase is about 0.08. The chemical compositions of the α- and β-phases obtained by EDX analysis are presented in Table III, where each data represents an average of ten measurements. The range of compositional variation in the β-phase is also given in Table III, due to the large variation. These results indicate that α-phase is rich in aluminium and contains practically no iron (below the detectability of the EPMA equipment), and that there is an enrichment of vanadium and iron in the β-phase. The composition for α-phase can be considered reasonably accurate while that for the β-phase is more approximate because the diameters of some of the β-grains are smaller than the interaction volume of the electron probe during the analysis. In fact, the actual concentration of vanadium and iron in the β-phase should be higher than the data listed in Table III, and that of aluminium should be slightly lower than 3.24 wt %. In addition, a compositional variation in the β-phase has also been observed during the EDX analysis. The larger β-grains located at α-grain triple points seem to contain less β-stabilizer, while the smaller β-grains located at α-grain boundaries contain more β-stabilizers.

TABLE I Results of chemical analysis of the master Ti–6Al–4V alloy

	Ti	Al	V	Fe	C	N_2	O_2	H_2
wt %	Bal.	6.43	4.02	0.19	0.01	0.0075	0.205	0.002

TABLE II Results of impurity analaysis of Ti–6Al–4V alloy after melt-spinning and comminution process (wt %)

Process	C	N_2	O_2
Melt-spun fibre	0.015	0.009	0.230
Comminuted powder	0.020	0.014	0.310

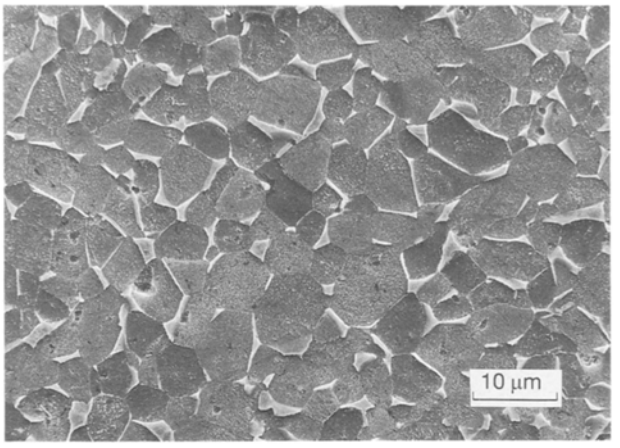

Figure 1 Scanning electron micrograph showing the microstructure of rapidly solidified Ti–6Al–4V alloy after HIPing at 900 °C, 300 MPa for 2 h. The white phase is β and the grey phase is α. The bright spots in the α-grains are due to the etching effect.

TABLE III EPMA results of phase composition in the consolidated Ti–6Al–4V alloy (wt %)

Phase	Ti	Al	V	Fe
α-phase	Balance	6.53	3.09	0.00
β-phase	Balance	3.24 (3.08–3.89)[a]	13.18 (10.15–14.25)[a]	1.61 (1.24–2.01)[a]

[a] Composition variation range of 10 β-grains.

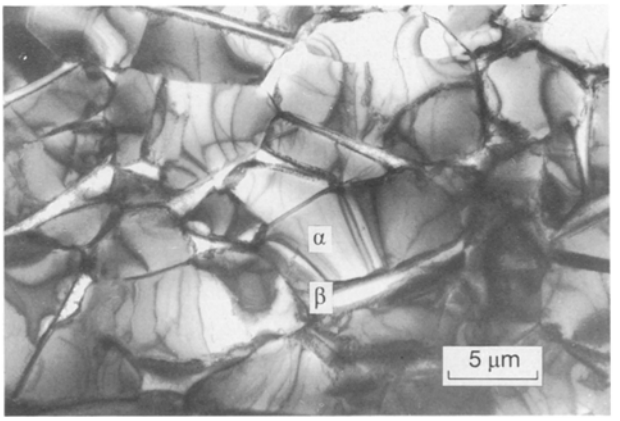

Figure 2 TEM bright-field image of rapidly solidified Ti–6Al–4V alloy showing the α + β structure.

A TEM bright-field image of the consolidated Ti–6Al–4V alloy is shown in Fig. 2. The α-grains are single crystals in which there is no sign of any transformation. Fig. 3 shows the detailed substructure of a large β-grain situated at a triple point of α-grains. Selected-area diffraction (SAD) of such β-grains revealed that direct $\beta \rightarrow \alpha$ transformation has occurred. Two typical SAD patterns from such β-grains with the electron beam parallel to $[0\,0\,1]_\beta$ and $[1\,1\,1]_\beta$ are shown in Fig. 4. These SAD patterns indicate that the α-phase in the β-matrix is Type 1 α, which was first observed by Rhodes and Williams [4] in Ti–Mo and Ti–Al–Mo alloys. Type 1 α obeys the well-known Burgers orientation relation between h c p α- and b c c β-phases, $(1\,1\,0)_\beta \| (0\,0\,0\,1)_\alpha$ and $\langle 1\,1\,1\rangle_\beta \| \langle 1\,1\,2\,0\rangle_\alpha$ [6]. There are 12 variants of the α-phase with this orientation relation possible in a single β-grain. The main characteristic of the $[0\,0\,1]_\beta$ zone axis pattern (Fig. 4a) is the presence of intense $\{1\,0\,\bar{1}\,0\}_\alpha$ reflections which occur between $\{1\,1\,0\}_\beta$ and $\{2\,0\,0\}_\beta$ reflections (see Fig. 4b). The $[1\,1\,1]_\beta$ zone axis pattern (Fig. 4c) is typified by the $\{1\,0\,\bar{1}\,0\}_\alpha$ reflections which occur between $\{1\,1\,0\}_\beta$ reflections (see Fig. 4d). A TEM dark-field image using the Type 1 α reflection is shown in

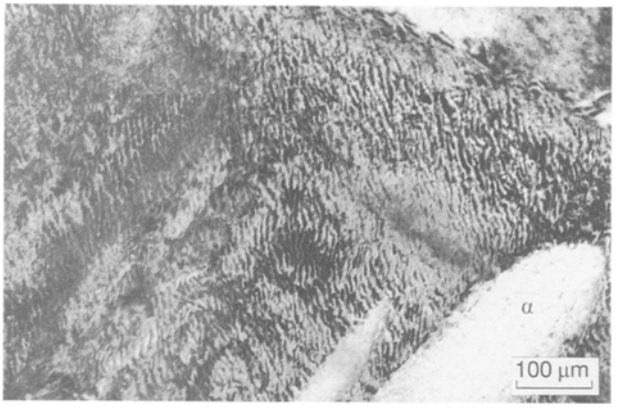

Figure 3 TEM bright-field image of a large β-grain showing the microstructure of the β-phase.

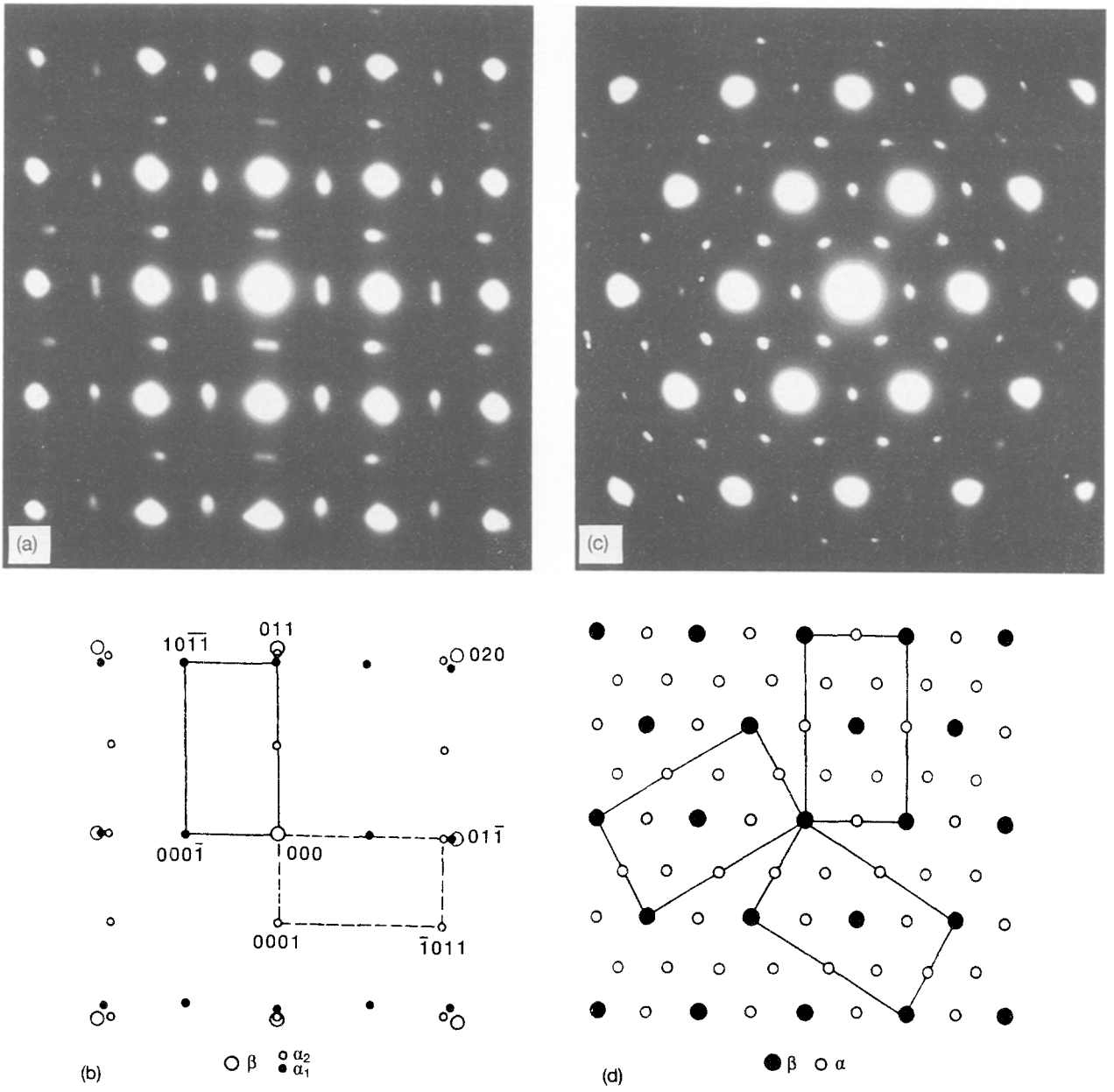

Figure 4 SAD patterns taken from a large β-grain showing the presence of Type 1 α which obeys the Burgers orientation relation between α- and β-phases. (a) $[0\,0\,1]_\beta$ zone axis pattern with two $\langle 1\,1\,\bar{2}\,0\rangle_\alpha$ patterns superimposed; (b) key to (a); (c) $[1\,1\,1]_\beta$ zone axis pattern with three $\langle 1\,1\,\bar{2}\,0\rangle_\alpha$ patterns superimposed; (d) key to (c).

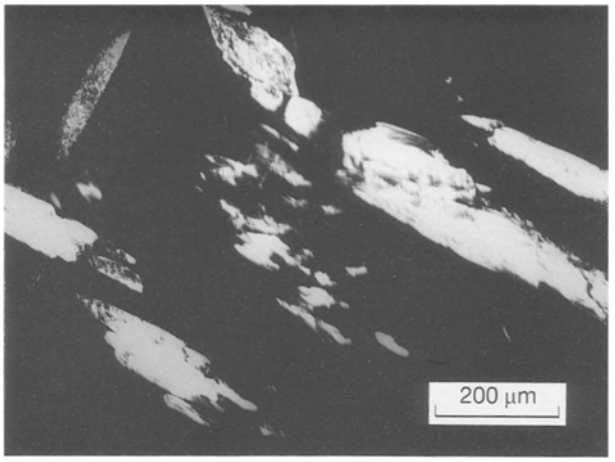

Figure 5 TEM dark-field image of the Type 1 α-phase.

Fig. 5. Type 1 α has a rod morphology with substructure in it.

Besides the presence of Type 1 α-phase, Type 2 α, which does not obey Burgers orientation relation [4], is also present in some of the β-grains, as evinced by the arched reflections in the SAD pattern in Fig. 6. The characteristic $\{1\,0\,\bar{1}\,0\}_\alpha$ reflections which appear in the Burgers orientation relation are not present in this pattern, and in addition there are arced precipitate reflections near the β-reflections which do not occur in the Burgers orientation relation.

A TEM bright-field image of a β-grain located at α-grain boundaries is presented in Fig. 7, which shows the typical features of a two-phase structure resulting from the spinodal decomposition, $\beta \rightarrow \beta + \beta'$, where β and β′ are coherent with each other [7]. In this composition-modulated two-phase microstructure, the β′-phase is lean of β-stabilizer (vanadium and iron), while the β-matrix is further enriched by β-stabilizers. The contrast which allows the coherent two-phase microstructure to be distinguished results mainly from the difference in thickness and relative absorption between the vanadium-rich β- and vanadium-depleted β′-phases. The vanadium-rich β-phase is preferentially thinned during the electropolishing and appears as the brighter regions in Fig. 7. It is well known that this compositional modulation takes place along the elastically soft directions [7]. In cubic crystal structures, the direction of modulation will be ⟨1 0 0⟩ or ⟨1 1 1⟩ depending on whether the elastic anisotropy factor $2C_{44} - C_{11} + C_{12}$ (where C_{ij} are the elastic constants) is positive or negative, respectively. According to experimentally determined elastic constants [8], the anisotropy factors for vanadium, niobium and molybdenum are all negative. It is reasonable to assume that the anisotropy factor for b c c titanium is also negative. Thus, the direction of the compositional modulation would be ⟨1 1 1⟩ in the present alloy. This has been confirmed by the experimental observations (see Figs 7 and 8). There are four variants possible in a single β-grain which has undergone spinodal decomposition. Different variants can be seen in Fig. 8, as exampled by variants A and B. The features of variants A and B indicate that β′-phase has a rod-shaped morphology, with the cross-section of the rods showing in variant B. Direct measurement on bright-field images in Figs 7 and 8 indicate that the wavelength, λ, of the compositional modulation in this alloy is about 5 nm. However, a conclusive identification of the spinodal decomposition of the β-phase by the appearance of the sideband using electron and X-ray diffraction techniques is difficult due to the very small difference between lattice parameters of two coherent b c c phases (β and β′) [9].

SAD patterns from the spinodally decomposed β-phase are shown in Fig. 9. Besides the strong b c c reflections, diffuse ω scattering along a variety of directions is present in these SAD patterns, which is characteristic of the initial stage of $\beta \rightarrow \omega$ transformation [10]. Occasionally, discrete spots corresponding to the ω-phase can be observed in SAD patterns taken from such β-grains located at α-grain boundaries. An example is given in Fig. 10 where the

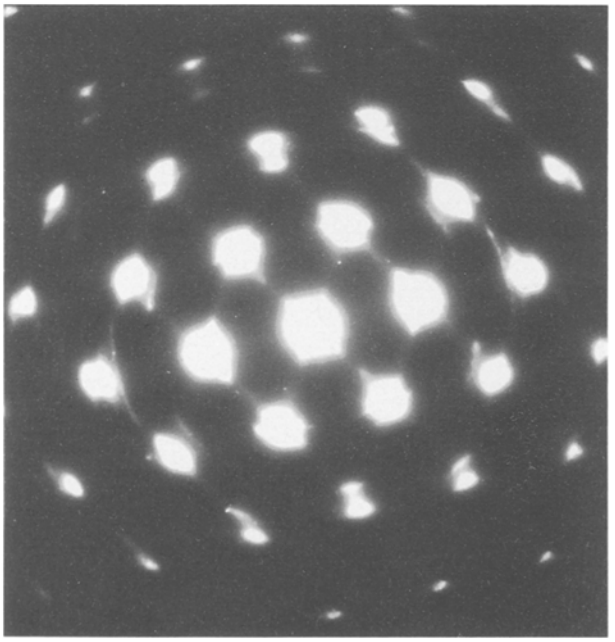

Figure 6 $[1\,1\,1]_\beta$ pattern taken from a large β-grain showing the presence of Type 2 α which does not obey the Burgers orientation relation between α- and β-phases and is characterized by the arched α-reflections in the vicinity of $\{0\,1\,1\}_\beta$ reflections.

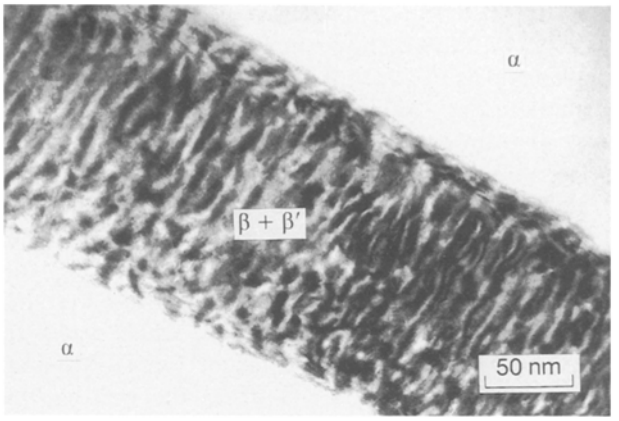

Figure 7 TEM bright-field image of a β-grain located at α-grain boundaries showing spinodal decomposition of the metastable β-phase into the β-stabilizer lean β′-phase and the β-stabilizer rich β-phase. The electron beam is close to $[1\,\bar{1}\,0]_\beta$, and the direction for compositional modulation is $\langle 1\,1\,1\rangle_\beta$.

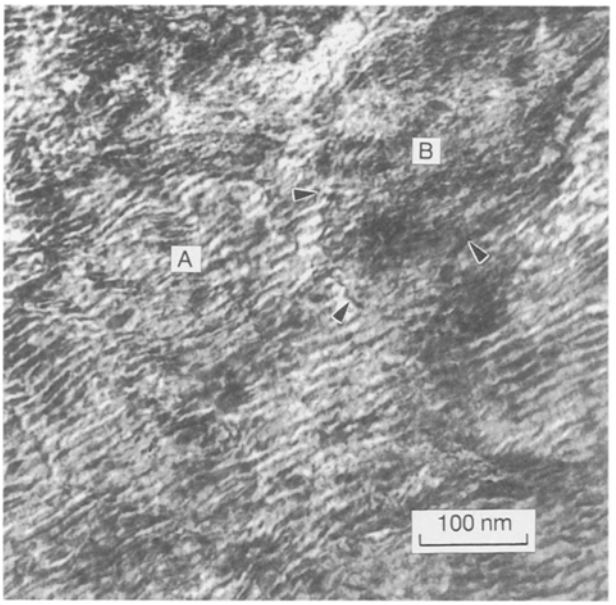

Figure 8 TEM bright-field image of a β-grain showing different domains of the β + β′ structure, for example domains A and B, with the domain boundaries being indicated by arrows. The electron beam is close to $[1\bar{1}0]_\beta$, and the direction for compositional modulation is $\langle 1\,1\,1\rangle_\beta$.

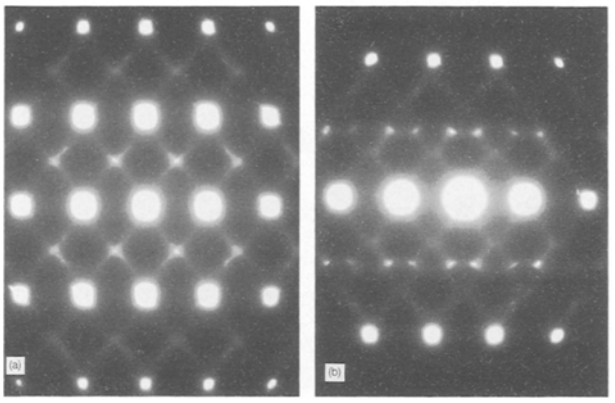

Figure 9 SAD patterns taken from the spinodally decomposed β-grains showing the diffuse ω scattering which is characteristic of the early stage of the β to ω transformation. (a) $[0\,1\,1]_\beta$; (b) $[\bar{1}\,3\,3]_\beta$.

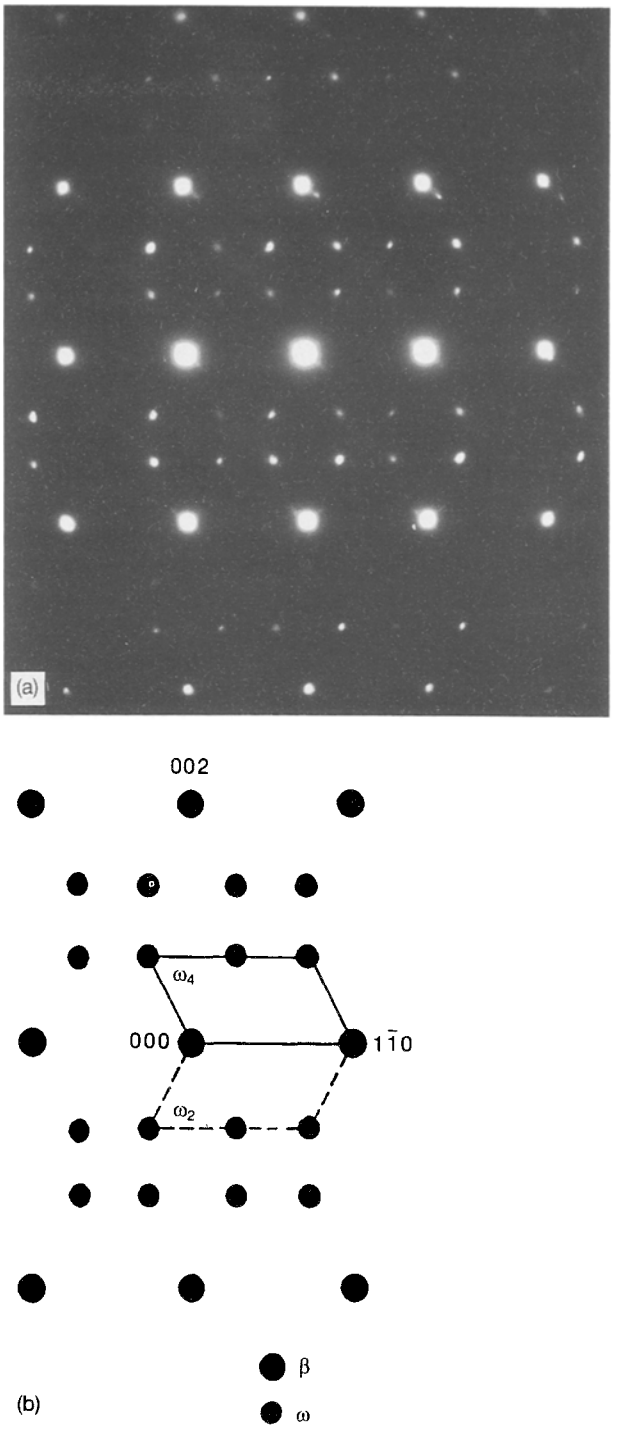

Figure 10 $[1\,1\,0]_\beta$ zone axis pattern taken from a spinodally decomposed β-grain showing the discrete spots from the ω-phase reflections, which are slightly shifted from the Bragg ω positions ($1/3\{2\,2\,2\}_\beta$ and $2/3\{2\,2\,2\}_\beta$) to positions of $0.36\{2\,2\,2\}_\beta$ and $0.64\{2\,2\,2\}_\beta$. (a) $[1\,1\,0]_\beta$ zone axis pattern: (b) key to (a).

electron beam is parallel to $[1\,1\,0]_\beta$. It is worth noting that the ω-reflections in Fig. 10a have been systematically shifted along the *c*-axis of the ω unit cell (parallel to $\langle 2\,2\,2\rangle_\beta$ directions) from the Bragg ω positions, i.e. $1/3\{2\,2\,2\}_\beta$ and $2/3\{2\,2\,2\}_\beta$ for $(0\,0\,0\,1)_\omega$ and $(0\,0\,0\,2)_\omega$ in the case of orientation variant ω_1, to positions of $0.36\{2\,2\,2\}_\beta$ and $0.64\{2\,2\,2\}_\beta$. This systematic shift of the ω reflections has also been observed in other titanium-base alloys, such as Ti–Fe, Ti–Mn and Ti–Cr, and has recently been discussed in detail by Sinkler and Luzzi [11]. The magnitude of the ω maxima shifts in SAD patterns depends on both the solute concentration and the identity of the solute. The amount of the ω maxima shift increases with increasing solute concentration beyond the limit for ω-phase formation [12]. In addition, the amount of the ω maxima shift also increases for a given solute concentration as the group number (in the Periodic Table) of the solute element increases [11]. A TEM dark-field image using the $(0\,0\,0\,1)_\omega$ reflection is shown in Fig. 11. The ω-phase appears as fine particles with a diameter around 5 nm. It is very interesting to see that ω particles tend to form parallel strings in the β-matrix. This result suggests that the ω-phase is transformed from the spinodally decomposed β′-phase which is lean of β-stabilizers, and gives further support to the occurrence of spinodal decomposition of metastable β-phase. Furthermore, in some of the β-grains, the coexistence of both ω- and Type 1 α-phases is also observed. This is shown by the $[1\,1\,0]_\beta$ zone axis pattern (Fig. 12a), which is a superimposition of

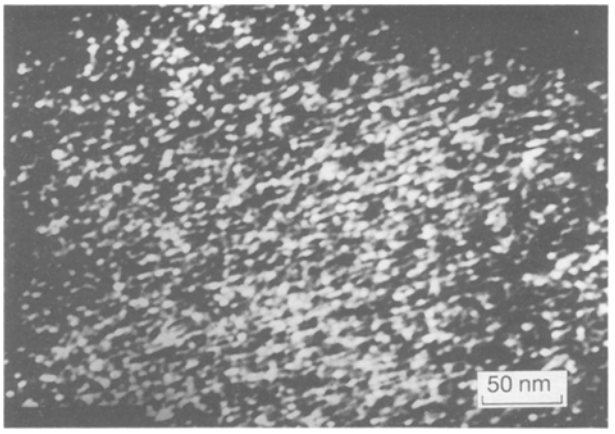

Figure 11 TEM dark-field image using $(0\,0\,0\,1)_\omega$ reflection showing the detailed morphology of the ω-phase. The ω-phase tends to form strings in the β-matrix.

two $\langle 0\,0\,0\,1\rangle_\alpha$ (α_1 and α_2) and two $\langle 1\,\bar{2}\,1\,0\rangle_\omega$ (ω_2 and ω_4) patterns, as schematically illustrated in Fig. 12b.

In addition to the presence of β′, Type 1 α, Type 2 α and ω-phase, there appears to be a further phase in the β-matrix, which cannot be identified as either the hcp α-phase, the orthorhombic α″-phase or bcc FeTi. Fig. 13a shows a typical SAD pattern of this unknown phase where the electron beam is parallel to $[\bar{1}\,1\,3]_\beta$, with the key to Fig. 13a being presented in Fig. 13b. In addition to the strong bcc reflections and the clear diffuse ω scattering, there are extra reflections present in Fig. 13a, which are located in the $1/2\{1\,1\,2\}_\beta$ positions. In some β-grains, selected-area electron diffraction indicates that two variants of the unknown phase are present in the β-matrix. One such SAD pattern is shown in Fig. 13c, which is a superposition of reflections from β-matrix, ω-phase, Type 1 α-phase and reflections from two variants of the unknown phase, as schematically illustrated in Fig. 13d. A TEM dark-field image using the reflection from the unknown phase indicated by an arrow in Fig. 13a is shown in Fig. 14. The unknown phase is present in the β-matrix as ellipsoidal particles with an average particle diameter about 5 nm, similar to the dimension of the ω-phase.

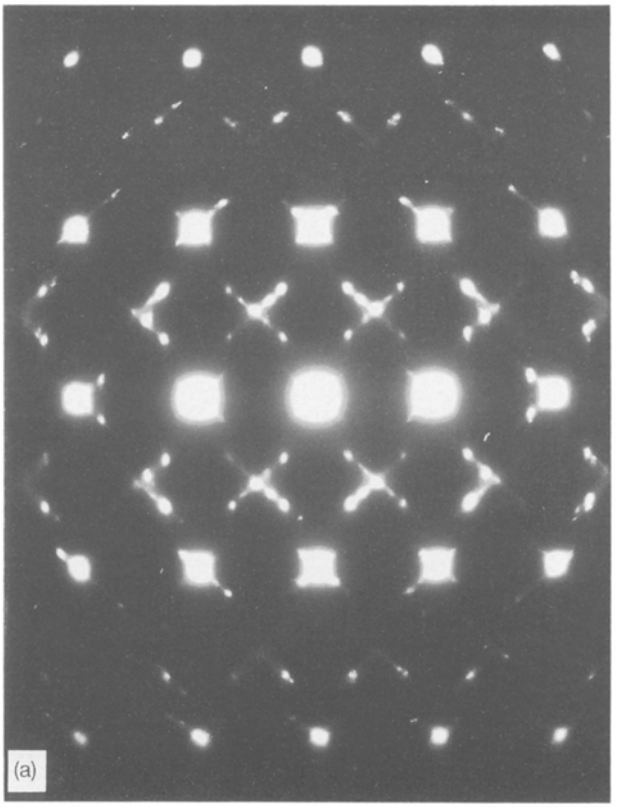

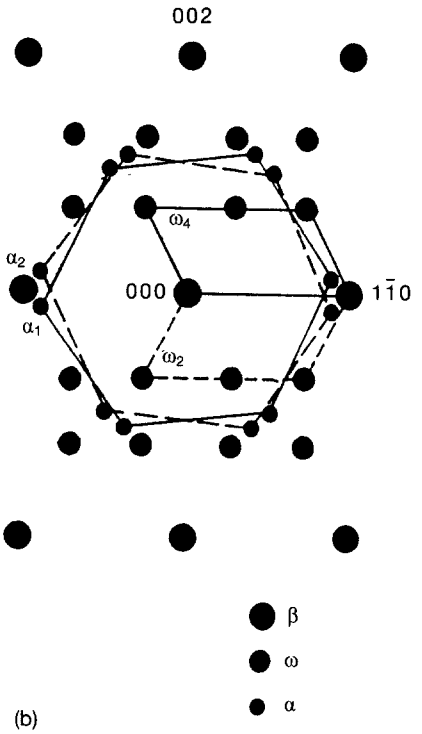

Figure 12 $[1\,1\,0]_\beta$ zone axis pattern taken from a spinodally decomposed β-grain showing the coexistence of ω-phase and Type 1 α. (a) $[1\,1\,0]_\beta$ zone axis pattern with two $\langle 0\,0\,0\,1\rangle_\alpha$ (α_1 and α_2) and two $\langle 1\,\bar{2}\,1\,0\rangle_\omega$ (ω_2 and ω_4) patterns superimposed; (b) key to (a).

4. Discussion

4.1. The chemical composition of the β-phase

The results from the EDX analysis indicate that the concentration of β-stabilizers (vanadium and iron) varies with β-grain size. The concentration of the β-stabilizers seems lower in larger β-grains than that in smaller ones. It was also noted that the β composition also varies from grain to grain with the similar grain size. The following factors may have contributed to this variation of composition:

(a) variation of the bulk composition during the melt-spinning process, i.e. the chemical composition of the melt-spun fibres obtained at the beginning of a production batch may be slightly different from that at the end of the same production batch;

(b) segregation of β-stabilizers during the solidification process from the wheel side (with the highest cooling rate) to free side (with the lowest cooling rate). EDX analysis of the cross-section of a 50 μm thick fibre indicated that the vanadium concentration at the wheel side is about 1 wt % higher than that at free side [13];

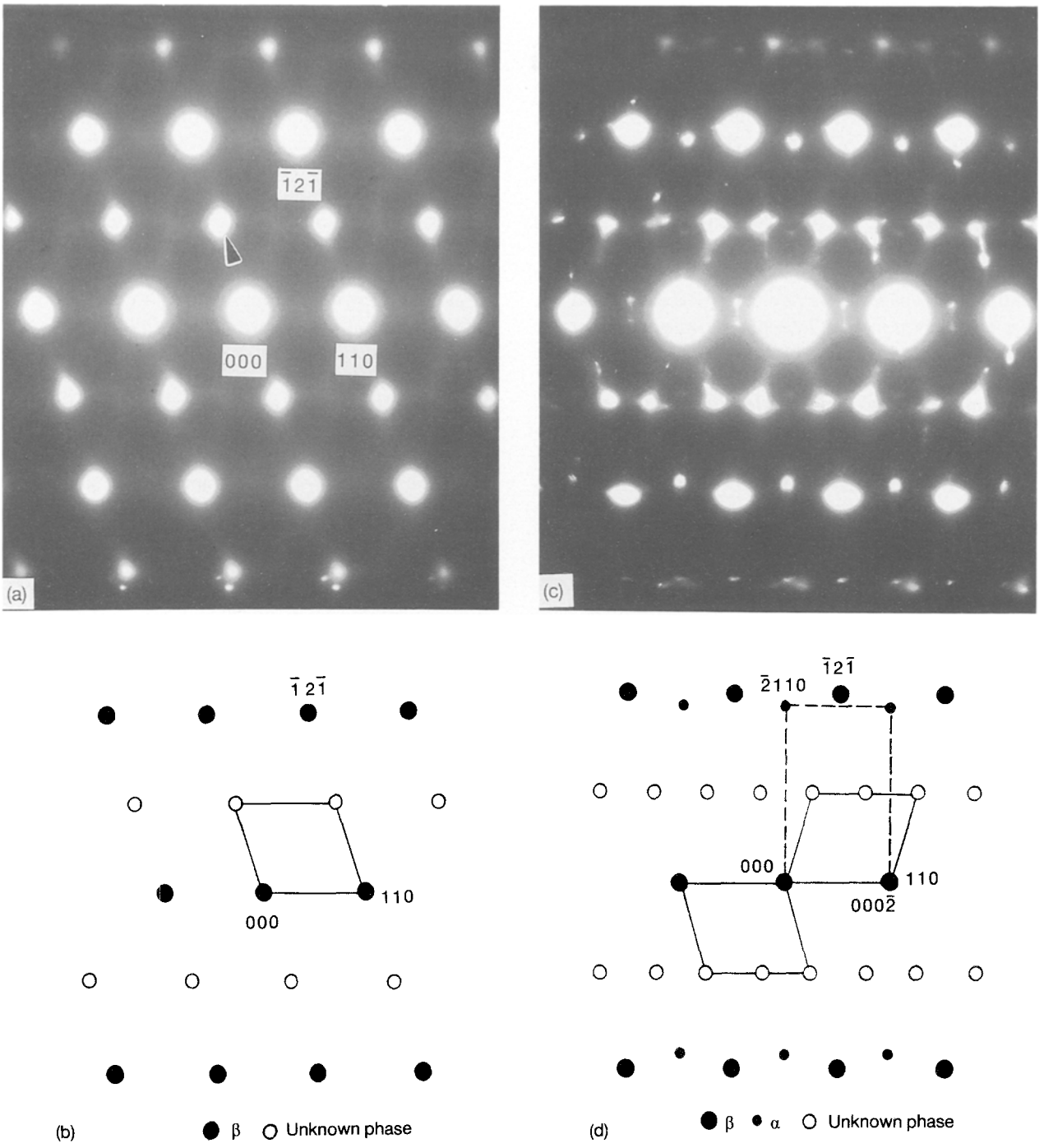

Figure 13 $[\bar{1}\,1\,3]_\beta$ zone axis pattern showing the presence of an unknown phase in the β-matrix, which is characterized by formation of $1/2\{1\,1\,2\}_\beta$ reflections. (a) $[\bar{1}\,1\,3]_\beta$ pattern superimposed with reflections from one variant of the unknown phase; (b) key to (a); (c) $[\bar{1}\,1\,3]_\beta$ pattern superimposed with a $[0\,\bar{1}\,1\,0]_\beta$ pattern and reflections from two variants of the unknown phase; (d) key to (c).

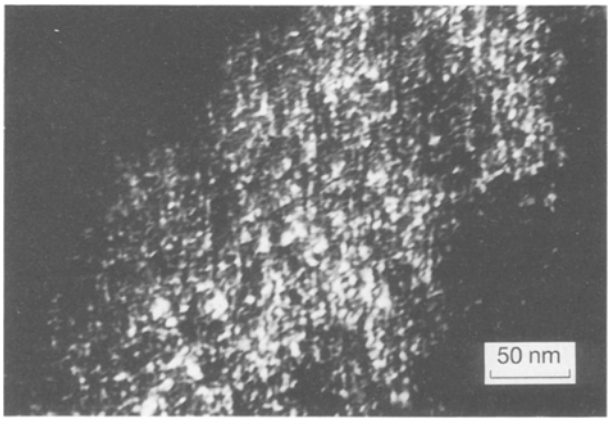

Figure 14 TEM dark-field image using reflection from the unknown phase as indicated in Fig. 13a by an arrow.

(c) insufficient time at HIPing temperature (2 h in this case) to produce macroscopic chemical homogeneity in the consolidated alloy.

It is believed that this variation in composition of the β-phase has a pronounced influence on the decomposition mode of the metastable β-phase and is responsible for much of the variation of the decomposition modes observed in the metastable β-phase, as will be discussed in later sections.

4.2. Formation of the ω-phase

Since its first discovery by Frost *et al.* [14] in aged Ti–Cr binary alloys, the ω-phase has received extensive study, initially because of its deleterious effects on mechanical and physical properties, but later also due

to the interests in the transformation mechanism. It is well known that the ω-phase can form by either quenching from high temperature (athermal ω-phase) or ageing at low temperature (isothermal ω-phase) [1, 2]. The ideal ω-phase has a hexagonal structure, belonging to space group D^1_{6H} (P6/*mmm*), and with a well-defined orientation relationship with the parent bcc β-phase, as first reported by Silcock [15]: $\{1\,1\,1\}_\beta \| (0\,0\,0\,1)_\omega$, $[1\,\bar{1}\,0]_\beta \| [1\,1\,\bar{2}\,0]_\omega$. Other structures of the ω-phase have also been reported in the literature, for example, trigonal ω, ordered ω, Zr_2Al-type ω and Ni_2Al-type ω (see review [16]). Recently there has been a renewed interest in ω-phase transformation due to the development of aluminide-based intermetallic materials, where an ordered B2 phase can transform into an ordered ω-phase during low-temperature ageing (e.g. [16–18]). The ω-phase has also been reported to occur in copper alloys [19–22], group IV transition metals with the β-stabilizer additions [23–25], aluminides such as NiAl and Ti3Al–Nb [26–28], iron-base alloys such as maraging steels [12, 29] and chromium-base alloys [30]. A common feature of these alloy systems, in which ω-phase occurs, is that there is either a bcc to hcp (e.g. titanium-base alloys) or bcc to fcc transformation (e.g. Fe–Ni maraging steels and Cr–Ni alloys) under equilibrium conditions. The ω-phase, therefore, is a metastable phase which occurs widely in alloy systems where a bcc-phase and a close-packed phase (either hcp or fcc) are in equilibrium.

Observation of the ω-phase in commercial Ti–6Al–4V alloy has been very rare [31–33]. In fact, the occurrence of ω-transformation in this alloy has been excluded by the argument that the concentrations of α-stabilizers (aluminium and oxygen) in the β-phase are sufficient to suppress the ω-phase formation [31, 33]. There appears to have been one report of the occurrence of ω-phase in quenched and aged Ti–6Al–4V alloy containing 0.116 wt % Fe and 0.15 wt % O [33].

The occurrence of ω-phase in the present Ti–6Al–4V alloy can be mainly attributed to the following three factors.

(a) Sufficient enrichment of β-stabilizers in the β-phase makes ω-phase formation thermodynamically favourable in competing with the martensitic transformation [34]. EDX analysis showed that vanadium and iron concentrations in the retained β-phase are more than 13.18 and 1.61 wt %, respectively. The effectiveness of iron as a β-stabilizer is about four times as much as that of vanadium on a weight per cent basis. Therefore, the equivalent vanadium concentration in the retained β-phase is over 20 wt %, which is sufficient to suppress the martensitic transformation [34–36]. This allows the ω-transformation to replace the martensitic transformation during the continuous cooling.

(b) A slow cooling rate from the HIPing temperature can create a favourable kinetic condition for the ω-phase formation. Recently, Moffat and Larbalestier [37] studied the effect of cooling rate from the annealing temperature to room temperature on the metastable β-phase decomposition mode in Ti–Nb binary alloys. They found that precipitation of the ω-phase was favoured by a slow cooling rate; in contrast, the formation of α″ martensite is favoured by a higher cooling rate. The present results in Ti–6Al–4V alloy support the above observation in Ti–Nb alloys. The cooling-rate dependence of the mode of metastable β-phase decomposition can be understood in terms of the role played by diffusion during the decomposition process. Martensitic transformation is diffusionless, therefore, diffusion has no influence on it, while the isothermal ω-phase transformation involves nucleation and growth. Slower cooling rate favours ω-phase formation by allowing the extent of diffusion required in the ω transformation process to be completed.

(c) The formation of a solute-lean β′-phase through the spinodal decomposition of the metastable β-phase favours the ω-phase formation in terms of composition depletion of β-stabilizers and lattice plane shift through the coherency strain. It has recently been confirmed by atom probe analysis that isothermal ω precipitates are depleted in all the alloying elements, both α- and β-stabilizers [38]. Therefore, the formation of a solute-lean β′-phase will reduce the amount of diffusion required by the formation of the ω-phase compared with its direct formation from the parent β-phase. In addition, the coherency strain between β and β′ phase will make both bcc structures distorted towards a trigonal structure by shifting the $\{1\,1\,1\}_\beta$ planes. Such a trigonal lattice is an intermediate structure between the bcc β and the ideal ω (hexagonal) structure. This point will be pursued further in Section 4.3.

4.3. Spinodal decomposition of the β-phase

The spinodal decomposition of the metastable β-phase in binary titanium-base alloys (including Ti–Nb and Ti–V) with sufficient β-stabilizer additions has been predicted theoretically by Kaufman and Nesor [39], Kool and Breedis [9] and more recently by Moffat and Kattner [40]. However, the experimental confirmation of this spinodal decomposition has not been conclusive [9, 37, 41, 42]. This can be attributed to the small difference of lattice parameter between the β- and β′-phases which makes the splitting of the β-phase reflection (sideband) in X-ray and electron diffraction measurements, practically unobservable.

In addition to the enrichment of β-stabilizers (vanadium and iron) in the β-matrix, the relatively high oxygen content in the present alloy may also contribute to the occurrence of spinodal decomposition of the metastable β-phase. Firstly, addition of a small amount of oxygen can effectively enhance the enrichment of β-stabilizers in the β-phase by raising the β solvus, as predicted theoretically by Saunders and Chandrasekaran [43], and consequently pushes the composition of the β-phase into the spinodal region. Secondly, oxygen addition can open up the metastable miscibility gap. Fuming and Flower [44] studied the effect of oxygen content on the β-phase

separation reaction in Ti–50V alloys with varying oxygen contents. They concluded that oxygen opens up the metastable miscibility gap in Ti–V system such that the phase separation is promoted at temperatures within the $\alpha + \beta$ phase field. This effect of oxygen can be understood by the suggestion made by Chernov and co-workers [45, 46], that oxygen is considered to increase the β interaction parameter (in the regular solution model) and, thus, opens up the metastable miscibility gap. The present Ti–6Al–4V alloy under investigation contains more than 0.31 wt % oxygen (see Table II), which may be sufficient to open up the metastable miscibility gap, and thus to allow the metastable spinodal decomposition to occur during continuous cooling.

The metastable β-phase decomposition process in the present Ti–6Al–4V alloy can be understood in terms of equivalent vanadium concentration in the metastable β-phase. During the continuous cooling from the HIPing temperature, enrichment of β-stabilizers occurs gradually. When the temperature and β-phase composition fall into the spinodal range, the decomposition takes place to form a β'-phase which is β-stabilizer lean and a β-phase which is enriched with β-stabilizers. With the continued cooling the ω-phase will form isothermally in the solute-lean β'-phase by nucleation and growth. However, the enrichment of β-stabilizers in some of the larger β-grains may not be enough to reach the range of spinodal decomposition, such β-grains will decompose by direct formation of the equilibrium α-phase. The α-phase formation will further enrich β-stabilizers in the β-matrix, and hence leads to the subsequent spinodal decomposition and ω-phase formation in the β-matrix, as evinced in Fig. 3.

A further relation between the spinodal decomposition and ω-phase transformation can be obtained by considering the crystallographical aspects of both transformations. On the one hand, when the spinodal decomposition occurs the composition modulation is along the elastic soft direction ($\langle 1\,1\,1\rangle_\beta$ in titanium alloys). Coherency between β and β' will distort both phases elastically to make them tend towards a trigonal lattice [7]. On the other hand, ω-phase is formed from the β-phase by collapsing a pair of neighbouring (1 1 1) planes to the intermediate position, leaving the next (1 1 1) plane unaltered, collapsing the next pair and repeating this process [21, 47]. This operation produces a structure of hexagonal symmetry which, in the limit of complete double-plane collapse, is called the "ideal ω", as described by Silcock [15]. However, the double-plane collapse in some alloy systems or at initial stage of this transformation may not be always complete, this will also produce a trigonal structure (trigonal ω, see [16]). The atomic plane arrangement in bcc, ideal ω and trigonal ω are schematically illustrated in Fig. 15. Therefore, the trigonal structure resulted from the coherency strain between β and β' phase in the spinodal should facilitate the ω-transformation from the β-stabilizer lean β'-phase.

A further thermodynamic assessment of the effects of aluminium and oxygen concentrations on the spinodal decomposition and the ω-phase formation in the Ti–Al–V system is currently in progress at Surrey University [17].

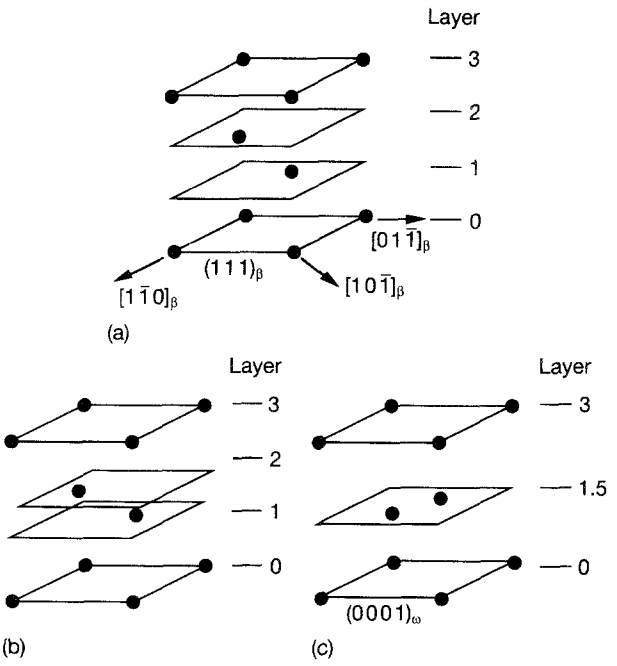

Figure 15 Schematic illustration of the atomic plane arrangement in (a) bcc lattice, (b) trigonal ω lattice, (c) ideal ω lattice (hexagonal).

5. Conclusions

1. During the continuous cooling the metastable β-phase can decompose by different modes, depending on the actual composition of the β-phase. Less enrichment of vanadium and iron in the β-phase will favour a direct formation of the equilibrium α-phase from the β-matrix, while the greater enrichment of vanadium and iron can lead to the spinodal decomposition of the metastable β-phase, resulting in the β-stabilizer lean β'-phase and the further enrichment of vanadium and iron in the β-matrix.

2. Upon further continuous cooling, the isothermal ω-phase can form from the spinodally decomposed β'-phase.

3. The occurrence of spinodal decomposition of the metastable β-phase in this alloy may have resulted from the following factors: (a) sufficient enrichment of vanadium and iron in the metastable β-phase; (b) slow cooling rate; (c) high oxygen content.

4. An unknown phase, which is characterized by formation of the $1/2\{1\,1\,2\}_\beta$ reflection in the SAD patterns taken from the β-matrix, has also been observed.

Acknowledgements

The authors thank Dr L. Chandrasekaran for his help with processing the Ti–6Al–4V alloy used in this investigation, and Dr P. Tsakiropoulos for his useful discussions. This work has been supported by the MOD, UK.

References

1. J. C. WILLIAMS, in "Titanium Science and Technology", Vol. 3, edited by R. I. Jaffee and H. M. Burte (Plenum Press, New York, 1973) p. 1433.

2. S. K. SIKKA, Y. K. VOHRA and R. CHIDAMBARAM, *Progr. Mater. Sci.* **27** (1982) 145.
3. E. L. HARMON and A. R. TROIANO, *Trans. ASM* **33** (1961) 43.
4. C. G. RHODES and J. C. WILLIAMS, *Metall. Trans.* **6** (1975) 2103.
5. Z. FAN, A. P. MIODOWNIK, L. CHANDRASEKARAN and M. WARD-CLOSE, *J. Mater. Sci.* **29** (1994) 1127.
6. W. G. BURGERS, *Physica* **1** (1934) 561.
7. J. W. CAHN, *Trans. Met. Soc. AIME* **242** (1968) 166.
8. R. F. S. HEARMAN, *Landolt-Bornstein* **1** (1966) 1.
9. M. K. KOOL and J. F. BREEDIS, *Acta Metall.* **18** (1970) 579.
10. J. C. WILLIAMS, D. de FONTAINE and N. E. PATON, *Metall. Trans.* **4** (1973) 2701.
11. W. SINKLER and D. E. LUZZI, *Acta Metall. Mater.* **42** (1994) 1249.
12. J. P. MORNOROLI, PhD thesis, University of Nancy, France (1974).
13. Z. FAN, unpublished work, University of Surrey, Guildford (1993).
14. P. D. FROST, W. M. PARRIS, L. L. HIRSCH, J. R. DOIG and C. M. SCHWARTZ, *Trans. ASM* **46** (1954) 231.
15. J. M. SILCOCK, *Acta Metall.* **6** (1955) 481.
16. C. P. CHANG and M. H. LORETTO, *Philos. Mag.* **63A** (1991) 389.
17. G. SHAO, PhD thesis in Progress, University of Surrey, Guildford (1994).
18. S. DJANARTHANY, C. SERVANT and O. LYON, *Philos. Mag.* **66A** (1992) 575.
19. M. de BONDT and A. DERUYTTERE, *Acta Metall.* **15** (1967) 993.
20. I. M. ROBERTSON and C. M. WAYMAN, *Philos. Mag.* **48A** (1983) 421.
21. *Idem, ibid.* **48A** (1983) 443.
22.
23. B. A. HATT and J. A. ROBERTS, *Acta Met.* **8** (1960) 575.
24. S. L. SASS, *Acta Metall.* **17** (1969) 813.
25. D. de FONTAINE, N. E. PATON and J. C. WILLIAMS, *ibid.* **19** (1971) 1153.
26. K. ENAMI, J. HASUNUMA, A. NAGASAWA and S. NENNO, *Scripta Metall.* **10** (1976) 879.
27. F. REYNAUD, *J. Appl. Crystallogr.* **9** (1967) 263.
28. R. STRYCHOR, J. C. WILLIAMS and W. A. SOFFA, *Met. Trans.* **19A** (1988) 225.
29. C. SERVANT, P. LACOMBE and M. GRIVEAU, *J. Mater. Sci.* **15** (1980) 859.
30. H. EZAKI, M. MORINAGA and N. YUKAWA, *Philos. Mag.* **57A** (1988) 651.
31. J. C. WILLIAMS and M. J. BLACKBURN, *Trans. ASM* **60** (1967) 373.
32. J. C. WILLIAMS, B. S. HICKMAN and D. H. LESLIE, *Met. Trans.* **2** (1971) 477.
33. A. LASALMONIE and M. LOUBRADOU, *J. Mater. Sci.* **14** (1979) 2589.
34. N. A. VANDERPUYE and A. P. MIODOWNIK, in "The Science, Technology and Applications of Titanium" (edited by R. I. Jaffee and H. M. Burte) (Pergamon Press, New York, 1970) p. 719.
35. P. PIETROKOWSKY and P. DUWEZ, *Trans. AIME* **194** (1952) 627.
36. T. SATO, S. HUKAI and Y. C. HUANG, *J. Aust. Inst. Met.* **5** (1960) 149.
37. D. L. MOFFAT and D. C. LARBALESTIER, *Met. Trans.* **19A** (1988) 1677.
38. L. HADJAJ, A. MENAND and C. MARTIN, quoted by N. E. Paton and H. L. Fraser, in "Proceedings of Sixth World Conference On Titanium", Vol. 3 edited by P. Lacombe, R. Tricot and G. Beranger (Societe Francaise de Metallurgie, France, 1988) p. 1469.
39. L. KAUFMAN and H. NESOR, in "Titanium Science and Technology", Vol. 2, edited by R. I. Jaffee and H. M. Burte (Plenum Press, New York, 1973) p. 773.
40. D. L. MOFFAT and U. R. KATTNER, *Met. Trans.* **19A** (1988) 2389.
41. G. H. NARAYANAN and T. F. ARCHBOLD, *Scripta Metall.* **4** (1970) 873.
42. O. LYON, C. SEVERAC and C. SERVANT, *Philos. Mag.* **48A** (1981) 825.
43. N. SAUNDERS and L. CHANDRASEKARAN, *J. Phase Equil.* **13** (1982) 612.
44. W. FUMING and H. M. FLOWER, *Mater. Sci. Tecnhol.* **5** (1989) 1172.
45. D. B. CHERNOV and A. YA. SHINAYAEV, *Russ. J. Phys. Chem.* **49** (1975) 445.
46. D. B. CHERNOV, V. V. MOLOKANOV, P. B. BUDBERG and A. YA. SHINYAEV, in "Titanium and Titanium Alloys", Vol. 2, edited by J. C. Williams and A. F. Belov (Plenum Press, New York, 1982) p. 1307.
47. D. DE FONTAINE, *Acta Metall.* **18** (1970) 275.

Received 28 April
and accepted 27 May 1994